Chinese Chemical Letters 35 (2024) 109448

Contents lists available at ScienceDirect

Chinese Chemical Letters

journal homepage: www.elsevier.com/locate/cclet

Long-lifespan thin Li anode achieved by dead Li rejuvenation and Li dendrite suppression for all-solid-state lithium batteries

Xuejie Gao[a,1], Xinyang Chen[a,1], Ming Jiang[c], Hanyan Wu[a], Wenfeng Ren[a], Xiaofei Yang[b,*], Runcang Sun[a,*]

[a] Center for Lignocellulosic Chemistry and Biomaterials, College of Light Industry and Chemical Engineering, Dalian Polytechnic University, Dalian 116034, China
[b] Division of Energy Storage, Dalian National Laboratory for Clean Energy, Dalian Institute of Chemical Physics, Chinese Academy of Sciences, Dalian 116023, China
[c] Institute of Physical Science and Information Technology, Anhui University, Hefei 230601, China

ARTICLE INFO

Article history:
Received 9 November 2023
Revised 7 December 2023
Accepted 20 December 2023
Available online 22 December 2023

Keywords:
Synergistic effect
In-situ Li_3Ga alloy
Suppress Li dendrite
Dead lithium regeneration
All-solid-state lithium metal batteries

ABSTRACT

Solid polymer electrolytes (SPEs) are considered to be one of the most promising systems applied in all-solid-state lithium metal batteries (ASSLMBs) on account of their chemical and electrochemical robustness, mechanical stability, cost-effective and scalable manufacturing techniques. Lately, significant endeavors have been directed towards mitigating the formation of the Li dendrite in SPE-based ASSLMBs, while research on the inactive lithium in the forms of the solid-electrolyte interface has been rarely reported. Herein, a bi-functional GaI_3 additive is developed for *in-situ* generating Li_3Ga alloy for suppressing Li dendrite growth, as well as I_3^- in recovering dead lithium. Relying on the density functional theory (DFT) results, the Li atom prefers to deposit on the Li_3Ga surface and then guide uniform Li deposition, while the I_3 species features a relatively lower lowest unoccupied molecular orbital (LUMO) energy level (-2.12 eV), meaning a higher electron affinity, which is beneficial for reviving inactive lithium to counterbalance the loss of lithium. As a result, in comparison to cells employing pure PEGDME-based electrolytes, the Li-Li symmetric cells utilizing GaI_3-containing solid-state electrolyte exhibited a cycling life nearly 30 times longer at a current density/capacity of 0.2 mA/cm^2, 0.2 mAh/cm^2. The full batteries of LFP//1%GaI_3-SPE//40 μm Li delivered a noteworthy capacity retention of 82% after 1300 cycles at a rate of 1 C.

As advanced energy storage system surpasses conventional lithium-ion batteries (LIBs), all-solid-state lithium metal batteries (ASSLMBs) are highly anticipated for meeting the requirements of electric vehicles and energy storage devices because of their high-energy-density and optimal safety features [1–6]. The incorporation of metallic lithium anodes and non-flammable solid-state electrolytes (SSEs) confers upon them remarkably enhanced energy density and safety [7–10]. Among the array of SSE systems available, solid polymer electrolytes (SPEs) have emerged as one of the most popular systems on account of their chemical and electrochemical robustness, excellent mechanical performance and scalable manufacturing techniques [11,12]. However, the practical implementation of SPEs is subject to several obstacles. During cycling, the volume variation of Li exposes the solid electrolyte interphase (SEI) to repetitive fracture and reformation, which leads to the uninterrupted consumption of reactive Li and electrolyte, along with the buildup of inactive Li, consequently limiting the cycling lifespan and contributing to a reduced Coulombic efficiency (CE) [13,14]. Moreover, the uncontrolled growth of Li dendrites and inadequate mechanical robustness of SPEs may cause internal short circuits and potential safety concerns [15–17].

In previous studies, most efforts have been dedicated to suppressing the Li dendrite, such as introducing inorganic fillers to bolster the mechanical strength of SPEs or designing porous hosts to reduce local current density [18–22]. However, there has been limited exploration concerning the inactive lithium (referred to as dead Li) manifested as the solid-electrolyte interface. Recent research has compellingly demonstrated that Li_2O, rather than LiF, predominates in the formation of the SEI layer on Li metal. The expansion and contraction variation during Li plating and stripping undermines the structural integrity and passivation capability of the Li_2O-dominated SEI, leading to the formation of inac-

* Corresponding authors.
E-mail addresses: yangxf@dicp.ac.cn (X. Yang), rcsun3@dlpu.edu.cn (R. Sun).
[1] These authors contributed equally to this work.

https://doi.org/10.1016/j.cclet.2023.109448
1001-8417/

tive Li [23–27]. This type of inactive Li serves as the primary cause of capacity degradation and insufficient lifespan, potentially posing a greater risk of contributing to thermal runaway compared to dendrites. This indicates that solving the problem of recovering dead lithium should be as important as suppressing dendrites, and by synergizing them a fundamental solution can be established for stabilizing ASSLMBs. Gallium(III) iodide (GaI_3) is composed of lithiophilic Ga^{3+} and strongly reducing I^-. Recent research has demonstrated that the reaction between Li^+ and Ga^{3+} can lead to the formation of the lithium-gallium (Li-Ga) alloy. This alloy displays high ion conductivity, excellent chemical robustness and good compatibility with lithium, endowed with significant advantages in suppressing Li dendrite [28–30]. For example, Zhou *et al*. proposed a novel dual-protection interface layer based on a Ga-Li alloy *via* a facile *in-situ* ion-exchange reaction, which features prolonged durability to effectively mitigate excessive consumption of active Li and ensure uniform Li deposition [31]. Wang *et al*. reported a Li_2Ga-carbonate polymer interphase layer aimed at simultaneously fulfilling multiple functions, including enhancing ion conduction, guiding Li^+ deposition, suppressing dendrite growth, and minimizing interface side reactions [32]. In addition, recent studies have shown that I^- can effectively revitalize Li which is electrochemically inactive in SEI. Jin *et al*. demonstrated the roles of the inert SEI in electrically isolated inactive Li metal and devised a Li rejuvenation technique based on iodine redox chemistry, which can effectively rejuvenate electrochemically inactive Li in both the inert SEI and electrically isolated Li metal debris [14].

Herein, GaI_3 was innovatively introduced into polyethylene glycol dimethyl ether (PEGDME) based SPEs to stabilize ASSLMBs. PEGDME, known for its advantageous properties as compared to other SPEs, offers improved compatibility with Li anode, as well as higher mechanical modulus and excellent solubility with GaI_3 [33]. Due to these properties, it is allowed to form an *in-situ* Li_3Ga alloy on the surface of the Li metal anode benefiting from the lithiophilic Ga^{3+} component, effectively suppressing the growth of Li dendrites and reducing undesirable side reactions between active Li and SPEs. Additionally, the strong reducing ability of I^- contributes to recovering dead Li back to the cathode for compensating the lithium loss. Relying on the X-ray diffraction (XRD) spectrum and density functional theory (DFT) results, Li-Ga alloy accords with the characteristic peaks of Li_3Ga and the Li atom prefers to deposit on Li_3Ga surface, facilitating uniform Li deposition, and thereby suppressing Li dendrites and achieving a stable cycling performance. The I_3 species, is characterized by a relatively low LUMO energy level (−2.12 eV) and a higher electron affinity, which is beneficial for reviving inactive lithium to counterbalance the loss of lithium. In addition, in view of the practical application, a Li foil of 40 μm is employed, which can efficiently improve the mass density to meet the commercial application [34]. As a result, in comparison to cells employing pure PEGDME-based electrolytes, the Li-Li symmetric cells utilizing GaI_3-containing solid-state electrolyte exhibited a cycling life nearly 30 times longer at a current density/capacity of 0.2 mA/cm^2, 0.2 mAh/cm^2 and achieved a cycling life of 320 h at current density/areal capacity of 0.2 mA/cm^2, 0.5 mAh/cm^2. Meanwhile, the full batteries of LFP//1%GaI_3-SPE//40 μm Li delivered a noteworthy capacity retention of 82% after 1300 cycles at a rate of 1 C.

In this study, the GaI_3-based SPE is prepared by introducing 1% GaI_3 powder into a PEGDME-based electrolyte. The PEGDME-based electrolyte design involves heating a blend of PEGDME and Li-salts to 120 °C until the complete melting of the polymers and dissolution of salts. Due to the presence of ethylene glycol and dimethyl ether moieties [35], PEGDME exhibits excellent solubility and coordination capability, allowing it to establish robust coordination interactions with GaI_3 and facilitate the dissolution of GaI_3 within PEGDME to form stable complexes. During battery cycling, the strong bonding interactions with lithium ions and gallium ions lead to the *in-situ* formation of a stable Li-Ga alloy on the surface of the lithium metal. The XRD spectrum demonstrates the metal alloy is Li_3Ga (Fig. S1 in Supporting information). The diffraction peaks at 20.9°, 25.1° and 32.4° of 2θ correspond to the (002), (101) and (110) crystal planes of Li_3Ga, respectively. The peaks of Li (JCPDS No. 15–0401) originate from the Li metal under the Li_3Ga alloy layer. The excellent chemical/electrochemical stability endowed by the alloy contributes to suppressing side reactions between lithium and the electrolyte, thereby minimizing additional lithium consumption. Furthermore, the favorable charge transfer kinetics ensure rapid lithium conduction and diffusion [36]. Moreover, because of its lithiophilic property, Li atoms preferentially nucleate uniformly and deposit on its surface selectively, thus suppressing the formation of Li dendrites. Furthermore, when the Li_2O-dominated SEI is undermined and leads to the formation of dead SEI and dead Li, the iodine ion in GaI_3 can effectively revitalize Li which is electrochemically inactive in it and replenish the lithium loss from two aspects. Firstly, iodine ions in the PEGDME-based electrolyte tend to exist in the form of triiodide ions (I_3^-, the prevalent state of iodine in the polar solvent [37]), which can corrode the Li_2O within the inactive SEI and convert into active lithium. This can be explained by the thermodynamically spontaneous reaction in Eq. 1.

$$3Li_2O + 3I_3^- = 6Li^+ + IO_3^- + 8I^- \quad (1)$$

Additionally, the $LiFePO_4$ (LFP) cathode provides a discharge plateau at 3.4 V under normal conditions [38], which exceeds the oxidation potential for the conversion of I^- to I_3^-. This can trigger the spontaneous reaction described in Eq. 2, directing the reutilization of lithium towards the cathode. We have tested the UV spectra of SPEs in LFP full cells before and after cycling. The rise of the peak of I_3^- in the UV spectra in Fig. S2 (Supporting information) can definitely prove this [39].

$$2Li^+ + 3I^- + 2FePO_4 = 2LiFePO_4 + I_3^- \quad (2)$$

Thanks to iodide ions, the facilitation of the two aforementioned steps enables the regeneration and recycling of inactive lithium within the dead SEI. As well as the presence of the Li_3Ga alloy, synergistic improves the stability and the cycling lifespan of the batteries. In contrast, in the pure PEGDME electrolyte, the haphazard nucleation of lithium on the surface of the Li anode leads to inhomogeneous lithium deposition (Scheme 1). With further lithium deposition, nonuniform lithium deposition becomes apparent, resulting in the creation of substantial layers of dead lithium.

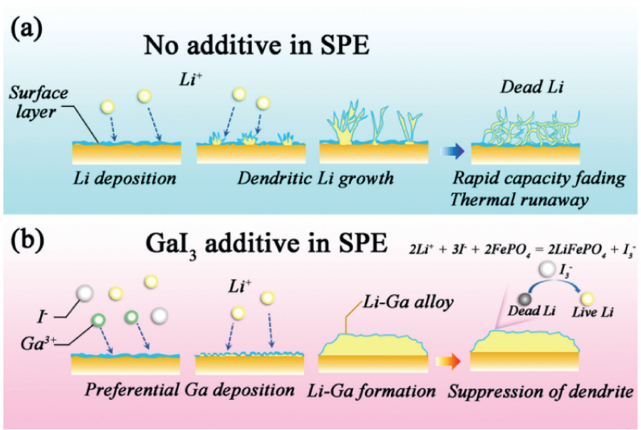

Scheme 1. Schematic showing the evolution of with/without GaI_3 additive in SPE upon electrochemical deposition/dissolution process.

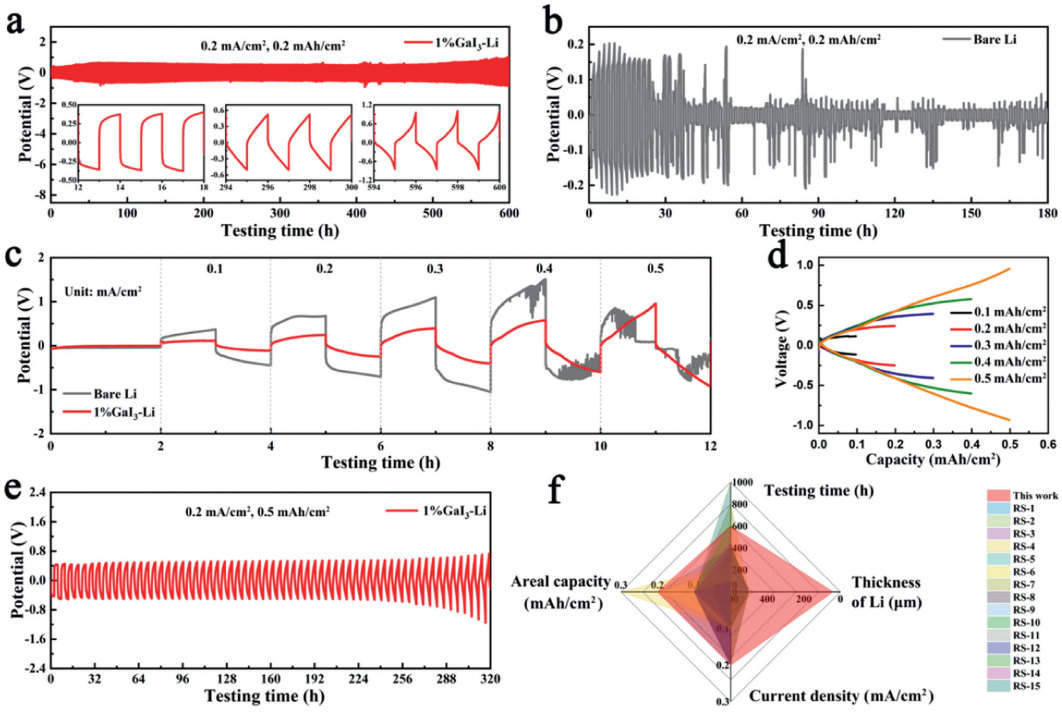

Fig. 1. Electrochemical performance of lithium symmetric cells with SPEs. (a, b) 1%GaI_3-Li and bare Li symmetric cells cycled at a current density of 0.2 mA/cm^2 and 0.2 mAh/cm^2. (c) Rate capability testing with current densities from 0.1 mA/cm^2 to 0.5 mA/cm^2. (d) Charge and discharge profile of 1%GaI_3-Li at different current densities. (e) 1%GaI_3-Li symmetric cell cycled at a current density and capacity of 0.2 mA/cm^2, 0.5 mAh/cm^2. (f) Comparison of this work with other lithium symmetric cells from literature.

This accumulation of inactive Li significantly increases the overpotential of the battery, eventually culminating in the occurrence of short circuits and safety issues.

To illustrate the pivotal role played by the GaI_3 additive in Li plating/stripping behavior, Li-Li symmetrical cells with 1%GaI_3-containing SPEs are assembled for evaluation, where pure PEGDME-based SPE is selected for comparison, labeled as 1%GaI_3-Li and bare Li, respectively. As illustrated in Fig. 1a, the 1%GaI_3-Li symmetric cell exhibits notably improved performance as compared to the bare Li symmetric cell (Fig. 1b). This enhancement can be credited to the *in-situ* creation of the Li_3Ga alloy, which functions as a shielding layer to maintain the structural integrity of the lithium metal electrode's surface. Moreover, it also serves as a supplier of I^- ions to recover dead Li for compensating the Li loss. In Fig. 1b, the performance of the bare Li symmetric cell is depicted at a current density of 0.2 mA/cm^2 with a capacity of 0.2 mAh/cm^2. Initially, it demonstrates an overpotential of approximately 200 mV during the early cycles. Subsequently, the overpotential experiences a rapid decline after only 26 h of cycling, followed by significant fluctuations during the next few cycles, indicating that a short circuit occurred. In contrast, as shown in Fig. 1a, although the overpotential is slightly higher as compared to its counterpart (bare Li), 1%GaI_3-Li symmetric cell exhibits a much longer cycling lifespan of 600 h, as opposed to the bare Li cell at the identical current density and capacity (0.2 mA/cm^2, 0.2 mAh/cm^2). The partial magnification (Fig. 1a) and the corresponding charge and discharge curves (Fig. S3 in Supporting information) further exemplify the stable Li plating and stripping behavior of the 1%GaI_3-Li symmetric cell. The improved cycling property and stability relative to the bare Li can be credited to the cooperative impacts of both the Li_3Ga alloy and the I^- ions. Specifically, the Li_3Ga alloy leverages its strong lithiophilicity to minimize the localized current density effectively by offering favorable sites for Li nucleation. Consequently, Li atoms are directed to grow uniformly on the surface of the electrode instead of disorganized aggregation during the plating/stripping process. The uniform deposition of Li inhibits the penetration of Li dendrites into the separator, thereby extending the cycle life with enhanced safety. Besides, the protective role of the Li_3Ga alloy layer can also safeguard the lithium metal surface from electrolyte corrosion to forbid uncontrollable side reactions between active Li and electrolyte. In terms of dead lithium that has already formed as part of the SEI during cycling, the I^- ions can corrode the Li_2O in the dead SEI and convert it into active lithium. This mechanism compensates for the Li losses, significantly enhancing the cycling performance of the batteries. Furthermore, to confirm the capability of the Li_3Ga alloy in suppressing Li dendrite formation, different rate performances of Li symmetric cells are also tested ranging from 0.1 mA/cm^2 to 0.5 mA/cm^2. As illustrated in Fig. 1c, the 1%GaI_3-Li symmetric cell exhibits consistently lower overpotential in comparison to the bare Li symmetric cell across all current densities. Notably, at a current density of 0.5 mA/cm^2, the 1%GaI_3-Li symmetric cell demonstrates favorable plating/stripping behavior, maintaining a low overpotential around at 1 V. The observation is substantiated by the corresponding voltage profile presented in Fig. 1d. As the current density escalates from 0.1 mA/cm^2 to 0.5 mA/cm^2, the rise of the voltage follows an ordered pattern, aligning closely with the aforementioned curves. It is worth noting that the bare Li symmetric cell experiences significant fluctuations when the current density is increased to 0.4 mA/cm^2, followed by a sudden drop in overpotential, indicating the irregular Li deposition and the short circuits under high current density. Moreover, the cycling performance of the 1%GaI_3-Li symmetric cell is further investigated at an elevated areal capacity of 0.5 mAh/cm^2 (Fig. 1e). As anticipated, the 1%GaI_3-Li symmetric cell maintains stable plating/stripping behavior at a high areal capacity for 320 h, as also evidenced by the corresponding charge/discharge curves (Fig. S4 in Supporting information). Undoubtedly, the comprehensive performance of 1%GaI_3-Li symmetric cell outperforms other SPE-based cells from previous publications across multiple metrics, encompassing operating current density, areal capacity, cycling lifespan and the thickness of Li

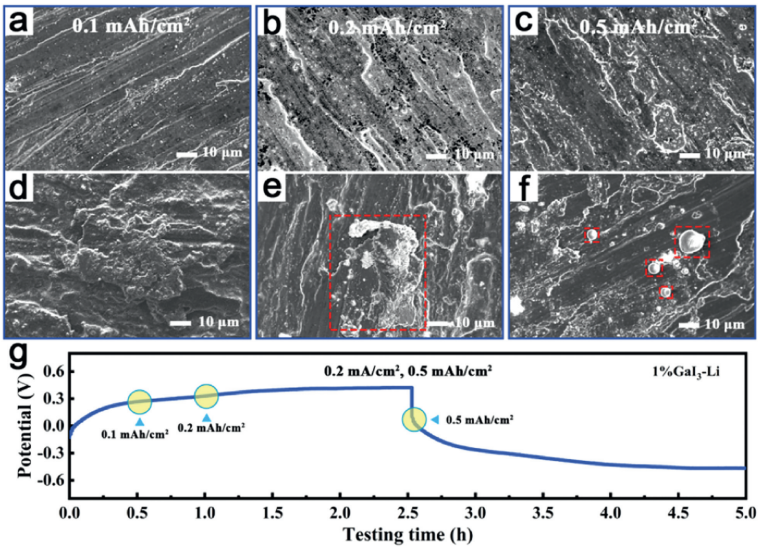

Fig. 2. SEM images of surface morphology evolution of 1%GaI_3-Li and bare Li anode after (a, d) 0.1 mAh/cm^2, (b, e) 0.2 mAh/cm^2, (c, f) 0.5 mAh/cm^2 of Li deposition. (g) The voltage profile indicated the Li plating state at a current density of 0.2 mA/cm^2, corresponding to (a)-(f).

foil. These are summarized and listed in Fig. 1f and Table S2 (Supporting information). Therefore, we firmly believe that this work sets a promising foundation for advancing SPE-based ASSLBs.

In order to obtain insights into the Li deposition behavior within the 1%GaI_3-Li and bare Li symmetric cells, SEM analysis is employed to examine the surface morphology of the Li anodes at various cycling capacities. Before conducting SEM analysis on electrodes, both the 1%GaI_3-Li and bare Li symmetric cells are disassembled in an Ar-filled glove box and then immersed into a DME solution for 12 h to eliminate any residual SPEs. As illustrated in Figs. 2a-f, the cells are subjected to discharging for durations of 0.5, 1, and 2.5 h under a controlled current density of 0.2 mA/cm^2, corresponding to areal capacity of 0.1, 0.2, and 0.5 mAh/cm^2. And Fig. 2g shows the corresponding testing time-potential curves. As illustrated in Fig. 2a, it can be observed that the anode surface of the 1%GaI_3-Li symmetric cell under 0.1 mAh/cm^2 presents a homogeneous Li deposition and a smooth surface due to the *in-situ* formation of the Li_3Ga alloy. The lithiophilic nature of Li_3Ga alloy contributes to offering preferential sites for Li nucleation, thus inducing selective nucleation and uniform Li deposition across the electrode surface. Conversely, the anode surface of the bare Li symmetric battery displays agglomeration of Li due to unordered deposition after cycling for 0.5 h. When the areal capacity is controlled to 0.5 mAh/cm^2 (Fig. 2e). With further Li plating, the preferential nucleation of lithium atoms at defects becomes more pronounced. This results in elevated local current density at these defect sites, further irregular deposition and increased agglomeration of lithium on the bare Li anode surface. Moreover, the initial formation of dendrites can also be observed. On the contrary, the 1%GaI_3-Li symmetric cell consistently maintains a flat surface of anode due to the uniform Li deposition and no evident Li agglomeration can be observed. This observation further underscores the pivotal role of the Li_3Ga alloy. After extending the Li plating time to 2.5 h, the bare Li anode exhibits an extremely rough surface, accompanied by significant lithium agglomeration. This can be credited to the uneven distribution of Li and the formation of inactive Li, causing a significant risk of short-circuit and compromised cycling performance at elevated areal capacity. However, as shown in Fig. 2c, the 1%GaI_3-Li symmetric cell still maintains a consistently homogeneous surface, with no obvious lithium agglomeration or accumulation of dead Li. This observation serves to emphasize the essential role that iodide ions play in the regeneration of dead lithium throughout the cycling process. The above distinctions in Li plating/stripping behavior between the 1%GaI_3-Li and bare Li symmetric cell further underscore the synergistic impact of Li_3Ga alloy in inhibiting Li dendrite growth and the iodide ions in rejuvenating dead lithium.

To additionally emphasize the crucial role of the GaI_3 additive, we investigate the electrochemical property of $LiFePO_4$ (LFP)-based ASSLMBs assembled with 1%GaI_3-containing SPE and pure PEGDME-based SPE as comparative samples. Figs. 3a and b show the design of the ASSLMB, where the two distinct SPEs are interposed between the LFP cathode and Li anode. Regarding the Li metal anode, the utilization of a 40 μm-thick Li foil is employed to efficiently enhance the mass density to meet the commercial application requirements. Besides, in the design of the LFP cathode, the combination of a conventional blade casting method and innovative freeze-drying techniques is employed. The freeze-drying process yields vertically aligned LFP structures, leading to an increased density of Li^+ transport channels and a reduction in Li^+ transport tortuosity as compared to conventionally blade-cast LFP cathode. Consequently, this aids in facilitating the transportation of Li^+ ions during the operation of the ASSLMB. As shown in Figs. 3c-f, benefiting from the additive of the GaI_3, the LFP//1%GaI_3-SPE//40 μm Li cell displays lower resistance and more stable cycling performance than the bare Li full cell. For instance, the LFP//1%GaI_3-SPE//40 μm Li cell exhibits a lower ohmic resistance (R_s) of 40 Ω. Moreover, the charge transfer resistance (R_{ct}), a parameter closely associated with the activation energy of chemical reactions in the 1%GaI_3 full cell (237 Ω), represents only 26% of its comparison (885 Ω). This suggests accelerated electrochemical kinetics attributed to the additive of GaI_3. In addition, the full cells are evaluated under galvanostatic charge/discharge conditions at 0.2 C within voltage ranges from 2.5 V and 4.0 V. As depicted in Fig. 3c, the initial cycle of the 1%GaI_3 full cell demonstrates a comparable specific capacity contrasted with the bare Li full cell. However, the discharge capacity of the bare Li full cell experiences a decline in subsequent cycles, eventually leading to a short circuit at 52 h. This phenomenon could be attributed to the instability of the SEI and the formation of uncontrollable lithium dendrites during cycling, as well it can also be observed in the corresponding charge-discharge curves in Fig. S5 (Supporting information). In contrast, the 1%GaI_3 full cell exhibits stable cycling, maintaining a specific capacity of 125 mAh/g after 250 cycles, corresponding to a high-capacity re-

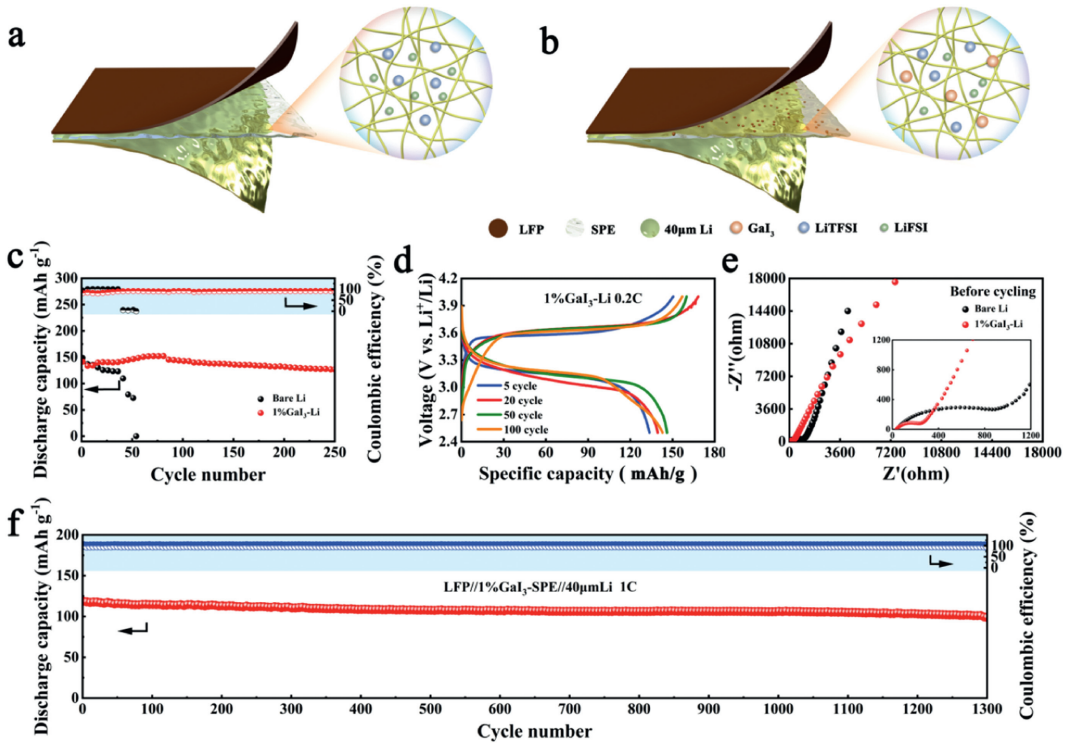

Fig. 3. Illustration and electrochemical performance of 1%GaI_3-Li and bare Li full cells with SPEs. (a, b) Schematic of bare Li (left) full cell and 1%GaI_3-Li (right) full cell with SPE. (c) The cycling performance at a rate of 0.2 C. (d) Charge and discharge profile of 1%GaI_3-Li at the rate of 0.2 C. (e) EIS plots of 1%GaI_3-Li and Bare Li full cells before cycling. (f) Long-term cycling performance of 1%GaI_3-Li at the rate of 1 C.

tention of approximately 88% and a negligible capacity decay of 0.04% per cycle. This enhanced performance is further confirmed by the corresponding charge/discharge curve (Fig. 3d) that the overpotential at the 5th, 20th, 50th, and 100th cycle does not increase significantly. The improved cycling behavior can be ascribed to the *in-situ* formation of the Li_3Ga alloy. The high conductivity of the Li_3Ga enhances Li^+ transport, while its lithiophilic nature ensures uniform Li deposition to suppress Li dendrite growth during the charging/discharging process, ultimately leading to superior cycling performance. Additionally, to showcase the long-term cycle ability of the 1%GaI_3-Li full cell, a higher rate of 1 C is tested (Fig. 3f). Remarkably, the LFP//1%GaI_3-SPE//40 μm Li cell starts with an initial capacity of 119 mAh/g and maintains a capacity of 98 mAh/g after over 1300 cycles, corresponding to a commendable 82% retention. This notable achievement could be attributed to the synergistic effect of the Li_3Ga alloy and iodide ions. The Li_3Ga alloy efficiently suppresses the growth of Li dendrites, while iodide ions effectively restore the dead Li, consequently directing the Li^+ ions to cycle back into the LFP cathode to revive the inactive lithium to counterbalance the loss of lithium. This confluence of effect, bolstered by the synergistic action of the Li_3Ga alloy and iodide ions, serves to stabilize the ASSLMBs and significantly enhance the cycling performance.

To further validate the experimental findings, we have conducted calculations to evaluate the adsorption strength and migration behavior of lithium atoms on the surfaces of both Li metal and Li_3Ga alloy. The computational specifics are available in Supporting information. The previous study has demonstrated that the Li(100) and Li_3Ga(111) surfaces exhibit the highest stability among Li metal and Li_3Ga alloy, respectively [31,40]. Thus, for the ensuing computations, the Li(100) and Li_3Ga(111) surfaces are selected to assess the adsorption strength related to the Li atoms. As illustrated in Figs. 4a and b, the assessment involves the top, hollow, and bridge adsorption sites. According to the results, we find that the Li atom exhibits a preference for adsorbing onto the hollow and bridge sites of the Li(100) surface (Table S1 in Supporting information). However, the adsorption energies of Li atoms on these sites display some difference (−1.36 and −1.31 eV, respectively). This result aligns consistently with the finding by Gaissmaier *et al.* [40]. As for the Li_3Ga(111) surface shown in Figs. 4c and d, the adsorption energy of hollow and bridge sites was calculated to be −1.76 eV. The Li atom is located at a similar hollow site after the structural relaxation, indicating that the bridge site is not stable. Moreover, the hollow site demonstrates greater ease for Li atom adsorption compared to the top site (Table S1). The values of adsorption in Table S1 represent the bonding strength between Li atoms and the substrate, where more negative values indicate stronger bonding strength. This suggests that there is a stronger interaction between Li atoms and the Li_3Ga(111) surface compared to the Li(100) surface which can explain why Li tends to deposit on the Li_3Ga alloy. We also conduct the Bader charge analysis to compare the charge transfer between the Li atom and the considered surface. As for the Li/Li_3Ga(111) interface, the Li atoms lose electrons, whereas the Ga atoms gain electrons. Especially, the adsorbed Li atom in the Li/Li_3Ga(111) interface loses about 0.84 |e|, which is more than the gained 0.71 |e| for the absorbed Li atom in the Li/Li(100) interface, indicating a propensity for the Li atom to favor deposition on Li_3Ga(111) surface.

In addition, a summary of the minimum energy pathways for Li atoms over Li(100) and Li_3Ga(111) surface is demonstrated in Figs. 4e and f. As shown in Fig. 4f, the energy barrier for Li diffusion across the Li(100) surface is 0.48 eV, which is calculated by comparing the energy difference between the initial and transition states. This result is consistent with the previously reported value of 0.47 eV [41]. As for the Li_3Ga(111) surface, the calculated energy barrier of Li diffusion is 0.39 eV, which is lower compared to the Li(100) surface. According to the aforementioned results, the Li_3Ga(111) surface possesses increased adsorption energy and

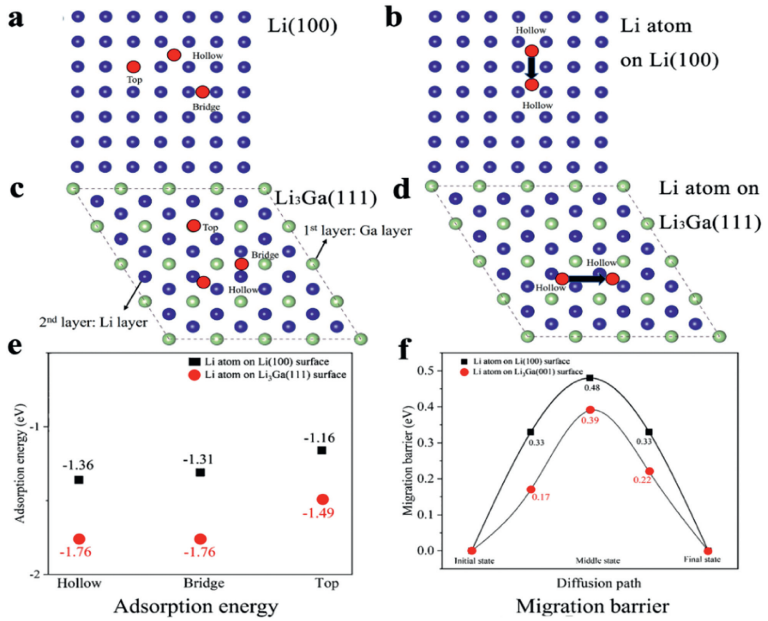

Fig. 4. (a, b) The top view of (a) Li(100) and (c) $Li_3Ga(111)$ surfaces and possible adsorption sites. (c, d) The possible diffusion path of Li atom on Li(100) and $Li_3Ga(111)$ surfaces. The blue and green spheres represent the Li and Ga atoms, respectively. The red sphere represents the possible adsorption sites, including the hollow, top and bridge sites. (e) The adsorption energy (eV) of Li atom on Li(100) and $Li_3Ga(111)$ surfaces. (f) The energy barrier (eV) of the Li atom migrating on the Li(100) and $Li_3Ga(111)$ surfaces.

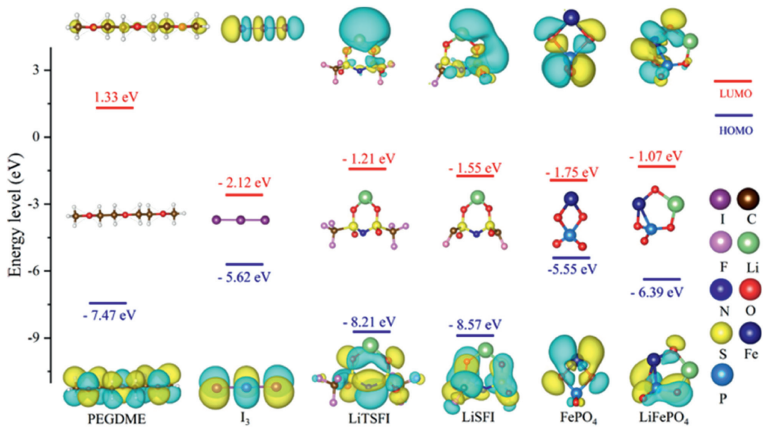

Fig. 5. LUMO–HOMO energy level diagrams of solutes and solvents. The blue and yellow surfaces represent the orbital wavefunction with opposite directions.

a reduced diffusion barrier, leading to the preference for Li atoms to deposit and rapidly diffuse on this special surface. Moreover, we also calculate the lowest unoccupied molecular orbital (LUMO) and the highest occupied molecular orbital (HOMO) of PEGDME, I_3, LiTSFI, LiSFI, $FePO_4$ and $LiFePO_4$ (Fig. 5). The results demonstrate that I_3 species possesses the lowest LUMO energy level (−2.12 eV), it means that a higher electron affinity and easy to reduce. This outcome demonstrates the advantageous role of the I_3 species in reviving inactive lithium to offset the losses in lithium.

In summary, we propose a synergistic strategy of using GaI_3 as an additive within SPEs. The GaI_3 additive can lead to the formation of the Li_3Ga alloy, which effectively suppresses the growth of Li dendrites. Additionally, the presence of iodide ions facilitates the recovery of inactive Li and compensates for lithium losses. Specifically, the Li_3Ga alloy promotes selective nucleation of Li and enhances Li^+ transport, contributing to stable cycling performance. Furthermore, iodide ions can direct the Li^+ ions back into the LFP cathode to counterbalance the loss of lithium and consequently increase the energy density output of ASSLBs. Based on DFT calculations, we find that Li atoms prefer to deposit on the Li_3Ga surface, which is beneficial for the rapid diffusion and the uniform deposition of Li. Simultaneously, through the calculation of HOMO and LUMO, we also find that the I_3 species possesses the lowest LUMO energy level (−2.12 eV), which means that a higher electron affinity and easy to reduce. This outcome demonstrates the advantageous role of the I_3 species in reviving inactive lithium to offset the losses in lithium. As a result, the 1%GaI_3-Li symmetric cell achieved almost 30 times longer cycling life at a current density/capacity of 0.2 mA/cm^2, 0.2 mAh/cm^2 as compared to the bare Li symmetric cell. Even at a higher areal capacity of 0.5 mAh/cm^2, the 1%GaI_3-Li symmetric cell maintained stable plating/stripping behavior for 320 h. Finally, in the context of the LFP cell employing the 1%GaI_3-containing SPE, a substantial capacity of 125 mAh/g was maintained after 250 cycles at 0.2 C. Even operating at a higher rate of 1 C, the LFP//1%GaI_3-SPE//40 μm Li cell still delivered noteworthy capacity retention of 82% after 1300 cycles. These results indicate that this work offers valuable insights into achieving stable cycling performance and high-power-density ASSLBs.

Declaration of competing interest

The authors declare that they have no known competing financial interests or personal relationships that could have appeared to influence the work reported in this paper.

Acknowledgments

This research was supported by the National Natural Science Foundation of China. (Nos. 22208039, 51961125207), the Basic Scientific Research Project of the Educational Department of Liaoning Province (No. LJKMZ20220878), the Dalian Science and Technology Talent Innovation Support Plan (No. 2022RQ036), and the Dalian Polytechnic University (Nos. 6102072202, 2023044).

Supplementary materials

Supplementary material associated with this article can be found, in the online version, at doi:10.1016/j.cclet.2023.109448.

References

[1] B.H. Zhang, Y.L. Liu, X.M. Pan, et al., Nano Energy 72 (2020) 104690.
[2] F. He, W.J. Tang, X.Y. Zhang, et al., Adv. Mater. 33 (2021) 2105329.
[3] Y.G. Lee, S. Fujiki, C. Jung, et al., Nat. Energy. 5 (2020) 299–308.
[4] Y.K. Sun, ACS Energy Lett. 5 (2020) 3221–3223.
[5] Y. Chen, K.H. Wen, T.H. Chen, et al., Energy Storage Mater. 31 (2020) 401–433.
[6] J.Y. Wu, L.X. Yuan, W.X. Zhang, et al., Energy Environ. Sci. 14 (2021) 12–36.
[7] C.H. Wang, T. Deng, X.L. Fan, et al., Joule 6 (2022) 1770–1781.
[8] D. Luo, M. Li, Y. Zheng, et al., Adv. Sci. 8 (2021) 2101051.
[9] C. Heubner, S. Maletti, H. Auer, et al., Adv. Funct. Mater. 31 (2021) 2106608.
[10] H.Y. Chen, M.X. Li, C.P. Li, et al., Chin. Chem. Lett. 33 (2021) 141–152.
[11] X.L. Zhao, P. Xiang, J.H. Wu, et al., Nano Lett. 23 (2023) 227–234.
[12] D.M. Reinoso, M.A. Frechero, Energy Storage Mater. 52 (2022) 430–464.
[13] C.C. Fang, J.X. Li, M.H. Zhang, et al., Nature 572 (2019) 511–515.
[14] C.B. Jin, T.F. Liu, O.W. Sheng, et al., Nat. Energy 6 (2021) 378–387.
[15] P.C. Zou, Y. Wang, S.W. Chiang, et al., Nat. Commun. 9 (2018) 464.
[16] F. Zhou, Z. Li, Y.Y. Lu, et al., Nat. Commun. 10 (2019) 2482.
[17] M.H. Ge, X.Y. Zhou, Y.P. Qin, et al., Chin. Chem. Lett. 33 (2021) 3894–3898.
[18] V.P. Hoang Huy, S. So, J. Hur, Nanomaterials 11 (2021) 614.
[19] W.Y. Zhang, Z. Su, S. Yi, et al., Small 19 (2023) 2207536.
[20] Z.Y. Hu, F. Ji, Y.F. Zhang, et al., Chem. Eng. J. 468 (2023) 143857.
[21] R. Pathak, K. Chen, F. Wu, et al., Energy Storage Mater. 41 (2021) 448–465.
[22] J.Y. Chen, Y.Z. Wang, S.J. Li, et al., Adv. Sci. 10 (2023) 2205695.
[23] Y.Z. Li, Y.B. Li, A. Pei, et al., Science 358 (2017) 506–510.
[24] M.J. Zachman, Z. Tu, S. Choudhury, et al., Nature 560 (2018) 345–349.
[25] X.F. Wang, G. Pawar, Y.J. Li, et al., Nat. Mater. 19 (2020) 1339–1345.
[26] Y.B. Xu, H.P. Wu, Y. He, et al., Nano Lett. 20 (2020) 418–425.
[27] S.J. An, J. Li, C. Daniel, et al., Carbon 105 (2016) 52–76.
[28] B. Han, D.W. Xu, S.-S. Chi, et al., Adv. Mater. 32 (2020) 2004793.
[29] C.L. Wei, L.W. Tan, Y. Tao, et al., Energy Storage Mater. 34 (2021) 12–21.
[30] B.W. Zhang, L. Ren, Y.X. Wang, et al., Interdiscip. Mater. 1 (2022) 354–372.
[31] Y. Zhou, J.M. Zhang, K. Zhao, et al., Energy Storage Mater. 39 (2021) 403–411.
[32] Z.P. Wang, S.Y. Xie, X.J. Gao, et al., Chin. Chem. Lett. 34 (2023) 108151.
[33] S. Choudhury, Z. Tu, A. Nijamudheen, et al., Nat. Commun. 10 (2019) 3091.
[34] Z.Y. Wang, L. Shen, S.G. Deng, et al., Adv. Mater. 33 (2021) 2100353.
[35] T. Yu, M.Q. Guo, S.M. Wen, et al., RSC Adv. 11 (2021) 13848–13852.
[36] R. Ruess, S. Schweidler, H. Hemmelmann, et al., J. Electrochem. Soc. 167 (2020) 100532.
[37] M. Tułodziecki, G.M. Leverick, C.V. Amanchukwu, et al., Energy Environ. Sci. 10 (2017) 1828–1842.
[38] B. Wang, T.F. Liu, A.M. Liu, et al., Adv. Energy. Mater. 6 (2016) 1600426.
[39] K. Lu, Z.Y. Hu, J.Z. Ma, et al., Nat. Commun. 8 (2017) 527.
[40] D. Gaissmaier, D. Fantauzzi, T. Jacob, J. Chem. Phys. 150 (2019) 041723.
[41] S. Liu, Q.Q. Zhao, X.Y. Zhang, et al., J. Mater. Chem. A 8 (2020) 17415–17419.